Identifying virulence determinants of multidrug-resistant *Klebsiella pneumoniae* in *Galleria mellonella*

Sebastian Bruchmann [a,b], Theresa Feltwell [b,c], Julian Parkhill [a], Francesca L. Short [b,c,d]

a Department of Veterinary Medicine, University of Cambridge, Cambridge, United Kingdom

b Wellcome Sanger Institute, Hinxton, United Kingdom

c Department of Medicine, University of Cambridge, Cambridge, United Kingdom

d Department of Molecular Sciences, Macquarie University, Sydney, Australia

Corresponding author:

Francesca L. Short, Department of Medicine, University of Cambridge, Cambridge, UK. Present address: ARC Centre of Excellence in Synthetic Biology, Macquarie University, Sydney, NSW 2109, Australia. Email: francesca.short@cantab.net; francesca.short@mq.edu.au

Abstract

Infections caused by *Klebsiella pneumoniae* are a major public health threat. Extensively drug-resistant and even pan-resistant strains have been reported. Understanding *K. pneumoniae* pathogenesis is hampered by the fact that murine models of infection offer limited resolution for the non-hypervirulent strains which cause the majority of infections. We have performed genome-scale fitness profiling of a multidrug-resistant *K. pneumoniae* ST258 strain during infection of the insect *Galleria mellonella*, with the aim to determine if this model is suitable for large-scale virulence factor discovery in this pathogen. Our results demonstrated a dominant role for surface polysaccharides in infection, with contributions from siderophores, cell envelope proteins, purine biosynthesis genes and additional genes of unknown function. Comparison with a hypervirulent strain, ATCC 43816, revealed substantial overlap in important infection-related genes, as well as additional putative virulence factors that may be specific to ST258. Our analysis also identified a role for the metalloregulatory protein NfeR (also called YqjI) in virulence. Overall, this study offers new insight into the infection fitness landscape of *K. pneumoniae* ST258, and provides a framework for using the highly flexible, scalable *G. mellonella* infection model to dissect the molecular virulence mechanisms of *K. pneumoniae* and other bacterial pathogens.

Keywords

Klebsiella pneumoniae, Galleria mellonella, TraDIS, Tn-seq, ST258

Introduction

Klebsiella pneumoniae is a gram-negative, capsulated bacterial pathogen responsible for a high proportion of hospital-acquired infections (Podschun and Ullmann 1998; Pendleton, Gorman and Gilmore 2013). Carbapenem-resistant *K. pneumoniae* is classified by the WHO as a critical priority for new drug development (Tacconelli *et al.* 2018). Classical *K. pneumoniae* (c*Kp*) causes a range of opportunistic infections (e.g. pneumonia, skin/soft tissue and catheter-associated urinary tract infections) in the elderly and immunocompromised, while hypervirulent *K. pneumoniae* (hv*Kp*) causes community-acquired invasive disease. Classical and hypervirulent *K. pneumoniae* can be distinguished by the presence of a specific virulence markers, or by their lethality in mice. Though

hypervirulent strains are a serious public health threat, the majority of *Klebsiella* disease burden is currently associated with classical strains (Wyres, Lam and Holt 2020). *K. pneumoniae* virulence factors include its protective polysaccharide capsule, O antigen, adhesive pili, capsule overproduction regulators and several different siderophores. Of these, the capsule overproduction genes and the siderophores aerobactin and salmochelin are hypervirulence markers that are absent from the majority of c*Kp* isolates.

Hv*Kp* strains are mouse-virulent with a lethal dose of less than10^6 colony forming units (cfu), while c*Kp* strains generally are not (Yu *et al.* 2007; Russo and Marr 2019; Russo and MacDonald 2020). The use of mouse models to study c*Kp* infections is typically limited to enumeration of surviving bacteria following challenge with very high inocula (for example, (Diago-Navarro *et al.* 2018; Palacios *et al.* 2018)). Such models capture intermediate points during self-resolving infections and may miss subtle virulence phenotypes. Furthermore, these models cannot easily be used in conjunction with the functional genomics approaches often used to identify infection-related genes *en masse* (e.g. Tn-seq, RNA-seq), as these methods require large numbers of bacteria to provide enough material for sequencing and avoid population bottlenecks (Cain *et al.* 2020). Due to these difficulties the majority of *K. pneumoniae* pathogenesis studies use infection of mice by hv*Kp* strains as the primary measure of virulence. Studying putative c*Kp*-relevant virulence genes in hv*Kp* strains may fail to identify relevant virulence activities, because mechanisms of pathogenesis vary between *K. pneumoniae* isolates (Xiong *et al.* 2015) and because even shared *K. pneumoniae* phenotypes can be underpinned by strain-specific gene sets (Dorman *et al.* 2018; Short *et al.* 2020)**.**

Alternative infection models for *K. pneumoniae* infections include *Dictyostelium discoideum, Drosophila melanogaster*, *Galleria mellonella*, *Caenorhabditis elegans*, zebrafish (reviewed in (Bengoechea and Sa Pessoa 2019)), and the *ex vivo* porcine lung (Dumigan *et al.* 2019). Of these models, the greater wax moth *Galleria mellonella* is by far the most established. *G. mellonella* larvae are susceptible to infection by both c*Kp* and hv*Kp* strains (Li *et al.* 2020; Russo and MacDonald 2020), and recapitulate many relevant features of mammalian infections (Insua *et al.* 2013). *G. mellonella* larvae used in research are not standardised, so published lethal doses in this model vary widely (e.g. those of MGH 78578 in (Insua *et al.* 2013; Wand *et al.* 2015), also reviewed in (Pereira *et al.* 2020). Despite this lack of standardisation, the virulence of different *K. pneumoniae* strains in *Galleria* broadly agrees with virulence in mice, though this relationship is not strong enough to reliably differentiate

between hv*Kp* and c*Kp* strains in the absence of other information (Li *et al.* 2020; Russo and MacDonald 2020). The flexibility of the *Galleria* model, and its susceptibility to c*Kp* infection, makes this a valuable animal model for high-throughput functional genomics studies of c*Kp*.

We have performed transposon directed insertion sequencing (TraDIS) to identify genes in *K. pneumoniae* RH201207 – a multidrug-resistant c*Kp* strain of the global, outbreak-associated clonal group ST258 – that contribute to *G. mellonella* infection, and compared the *in vivo* fitness requirements of this c*Kp* strain to that of the hv*Kp* strain ATCC 43816. Our results identify known virulence genes along with newly identified putative virulence factors, and we have validated the TraDIS screen with defined single-gene mutants. One gene of interest was the Nickel-dependent transcriptional repressor NfeR, which has not previously been linked to virulence in any species. An NfeR mutant showed reduced virulence and increased expression of a neighbouring ferric reductase gene – effects that were reversed by complementation – but, unexpectedly, could not be linked to any *in vitro* phenotypes. Overall, our results show that the *Galleria mellonella* model is well-suited to high-throughput functional genomics studies of c*Kp* strains, and suggest that even very subtle disruptions to metal homeostasis may be important during c*Kp* infections.

Material and Methods

Bacterial strains and culture conditions

Bacterial strains, TraDIS libraries, plasmids and oligonucleotides used in this work are listed in Table S1. *Klebsiella pneumoniae* RH201207 (ST258) and ATCC 43816 (ST493) were grown in LB medium at 37 °C with shaking for routine culture. Where necessary, antibiotics were added in the following concentrations: tetracycline 15 µg mL^{-1}, chloramphenicol 25 µg mL^{-1}. Viable counts of bacterial cultures were determined by serial dilution in PBS followed by spot-plating of the entire dilution series with technical duplicates.

Galleria mellonella infection experiments

Research-grade *G. mellonella* larvae (Biosystems Technology Ltd, UK) were kept at room temperature in the dark for a maximum of 7 days before use. Injections and haemolymph extractions were performed as described (Harding *et al.* 2013). For survival analyses, *K. pneumoniae* strains were grown to late exponential phase (OD_{600} = 1), harvested by

centrifugation, and resuspended in sterile PBS. 10 µL doses of diluted bacterial suspensions were injected into the right hind proleg of the larvae, and the infected larvae were incubated in the dark at 37 °C. Larvae were scored as dead when they were unresponsive to touch.

TraDIS infection experiments were performed in biological triplicate using previously reported high-density mutant libraries. Aliquots of frozen pooled transposon mutant libraries (minimum of 10^8 cells) were grown overnight, subcultured and grown to late exponential phase, then resuspended and diluted in PBS to an approximate density of 10^7 cfu mL^{-1}. Groups of larvae were injected with 10 µL prepared TraDIS library per larva (approx. dose 10^5 cfu) and incubated at 37 °C in the dark. Bacteria were extracted from infected *Galleria* as follows: haemolymph was recovered from all of the larvae in each group and pooled in 4 volumes of ice-cold eukaryotic cell lysis buffer (1 × PBS + 1 % Triton X-100) and the mixture was held on ice for ten minutes. Treated haemolymph was centrifuged at 250 × *g* for 5 minutes to pellet eukaryotic cell debris while leaving the majority of bacterial cells in the supernatant. The supernatant was centrifuged at 8000-10000 × *g* for 2 minutes to pellet bacterial cells, and bacteria were resuspended in 5 mL LB and outgrown at 37 °C to approx. OD_{600} of 1 in order to generate enough material for gDNA extraction and sequencing. The final post-infection time points were chosen as the time where there was visible melanisation of the majority of larvae in each group, but no reduction in the volume of recoverable haemolymph. This corresponded to a per-larva bacterial load of ~2×10^7 cfu.

Specific parameters for *G. mellonella* TraDIS infection experiments were as follows. RH201207: 20 larvae per group, 1.5×10^5 cfu inoculum, time points at 2 h post-infection (hpi) and 6 hpi, outgrowth periods 4 hours (2 hpi samples) and 1.5 hours (6 hpi samples); ATCC 43816: 12 larvae per group, 1.1×10^5 cfu inoculum, time point at 4 hpi, outgrowth period 2 hours.

Genome re-sequencing and annotation of RH201207

Genomic DNA of RH201207 was extracted using the MasterPure Complete DNA and RNA Purification Kit (epicentre) with DNA resuspended in 50 µL nuclease free water by carefully flicking the tube. Purity was checked on a NanoDrop spectrophotometer (260/280 of 2.01, 230/260 of 2.12) and quality and quantity assessed on a TapeStation (Agilent) with DIN of 9.7 and concentration of 36.9 ng μL^{-1}.

Nanopore 1D sequencing library was prepared using the genomic DNA by ligation sequencing kit SQK-LSK109 (Oxford Nanopore Technologies, ONT), barcoded using the barcoding extension kit EXP-NPB104 and sequenced on a GridION X5 using a R9.4.1 flow cell (ONT) together with five bacterial genomes from a different study. Bases were called with Albacore v2.0 (ONT) and adapter sequences were trimmed and sequencing reads de-multiplexed with Porechop v0.2.3 (https://github.com/rrwick/Porechop). Genome assembly was performed in combination with the previously described paired-end Illumina reads of RH201207 (Jana *et al.* 2017) accessible at the ENA (study PRJEB1730). The hybrid read set was assembled with Unicycler v0.4.7 (Wick *et al.* 2017) using the normal mode and assembly graphs were visualised with Bandage (Wick *et al.* 2015). The final assembly was annotated using Prokka v1.14.5 (Seemann 2014) with additional functional gene annotation by KEGG (Kanehisa and Goto 2000) and UniProt (The UniProt Consortium 2019). Plasmid replicons were identified with PlasmidFinder (Carattoli *et al.* 2014). Typing of the *Klebsiella* K- and O-loci was performed with Kaptive (Wick *et al.* 2018). Iron uptake genes were annotated with SideroScanner (https://github.com/tomdstanton/sideroscanner).

TraDIS sequencing and analysis.

Genomic DNA was extracted by phenol-chloroform extraction. At least 1 µg DNA per sample was prepared for TraDIS as described in (Barquist *et al.* 2016). Sequencing statistics and accession numbers are given in Table S2. Sequencing reads were mapped to the RH201207 or ATCC 43816 genomes using the Bio::TraDIS pipeline as described previously (Langridge *et al.* 2009; Barquist *et al.* 2016), with a 96 % mapping threshold, multiply-mapped reads discarded and one transposon tag mismatch allowed (script parameters: "-v --smalt_y 0.96 --smalt_r -1 -t TAAGAGACAG -mm -1"). Insertion sites and reads were assigned to genomic features with reads mapping to the 3' 10 % of the gene ignored, and between-condition comparisons were performed without read count filtering. Gene essentiality was determined by running tradis_essentiality.R (Barquist *et al.* 2016) on the combined gene-wise insertion count data of all three biological replicates. Essential or ambiguous-essential genes of the input samples (the initial transposon library) as defined by the Bio::TraDIS pipeline were excluded from further analysis. Gene functional categories were assigned to genes using EggNOG Mapper (Huerta-Cepas *et al.* 2017) and enrichment of clusters of orthologous groups (COG) was determined by two-tailed Fisher's exact test in R version 3.6.2 (R-function fisher.test) (R Core Team 2019).

Mutagenesis and complementation

Deletion mutants of *K. pneumoniae* RH201207 were generated by allelic exchange using vectors derived from pKNG101-Tc as described (Dorman *et al.* 2018). Transposon-insertion mutants of *K. pneumoniae* RH201207 were generated by subjecting the TraDIS mutant library to two rounds of density-gradient selection then identifying mutants by random-primed PCR as described (Short *et al.* 2020).

Klebsiella pneumoniae phenotypic tests

All quantitative phenotypic tests reported are from three biological replicates. Serum susceptibility was determined by incubation of late log-phase cells with 66 % normal human serum (Sigma-Aldrich) as described (Short *et al.* 2020). Siderophore production was visualised by the chrome azurol S assay (Schwyn and Neilands 1987; Louden, Haarmann and Lynne 2011) with the following measures to remove trace iron: glassware was soaked in 6 M HCL for two hours and rinsed three times with ultrapure water, and Casamino acid solution was treated with 27 mL 3 % 8-hydroxyquinoline in chloroform for 20 minutes, then the supernatant was removed, extracted once with a 1:1 volume chloroform, and filter-sterilised. Overnight cultures of *K. pneumoniae* strains were normalised to an OD_{600} of 0.5 prior to spotting on CAS agar, and plates were incubated at 37 °C for 48 hours. For qRT-PCR, total RNA was extracted from bacteria grown in LB medium to OD = 1 using a Qiagen RNeasy kit, and treated with TURBO DNase. Transcripts of *nfeF* and the *recA* housekeeping gene were quantified using a KAPA SYBR fast one-step qRT-PCR master mix according to the manufacturer's instructions. Three biological replicates and two technical replicates were performed, with 2.5 ng total RNA per reaction. Sensitivity to hydrogen peroxide was determined by diluting stationary phase cultures 1:100 in Mueller-Hinton II medium, then adding hydrogen peroxide (30 % v/v, Sigma-Aldrich) to a final concentration of 4-8 mM. Samples were incubated at 37 °C for 120 minutes before serial dilution and plating to enumerate surviving bacteria. Nickel toxicity and dipyridyl sensitivity tests were performed in a 96-well plate format with 100 µl volume per well and an initial cell density (seeded from overnight culture) of OD_{600} = 0.05. Nickel toxicity tests were performed in LB medium supplemented with nickel(II) sulfate hexahydrate (Sigma-Aldrich). Dipyridyl sensitivity tests were performed in M9 minimal medium supplemented with 0.2 % glucose, with the inoculum washed three times in M9 salts. Plates were sealed with air-permeable film and incubated with shaking for 18 hours at 37 °C prior to measurement of OD_{600}.

Availability of sequencing data

The TraDIS sequencing data is available in the European Nucleotide Archive (https://www.ebi.ac.uk/ena/browser/home) under the Study Accession No. PRJEB20200. Individual sample accession numbers are available in Table S2. Oxford Nanopore reads of RH201207 are available in the ENA repository under study accession number PRJEB40551.

Results and Discussion

TraDIS analysis of *G. mellonella* infection determinants in *K. pneumoniae* RH201207

Klebsiella pneumoniae RH201207 is a multidrug-resistant isolate of clonal group CG258 used in previous transposon insertion sequencing studies (Jana *et al.* 2017; Short *et al.* 2020). We first measured *K. pneumoniae* RH201207 infection parameters in *G. mellonella*. An inoculum of ~10^5 cfu was sufficient to kill the majority of infected larvae, with melanisation evident at 5 hours post infection. For TraDIS analysis, three groups of *G. mellonella* larvae were infected with replicate cultures of the *K. pneumoniae* RH201207 mutant pool, and we recovered and sequenced surviving bacteria from the larval haemolymph at 2 hpi and 6 hpi; the volume of haemolymph that could be recovered declined at later time points. Haemolymph was treated with detergent to lyse eukaryotic cells, then bacteria were recovered and grown in rich medium (Fig. 1A). This method allowed high recovery of infecting bacteria without antibiotic selection, while avoiding co-isolation of DNA from either the host or its microbiota. Viable counts were measured on infection and at each sampled time point, and showed approximately seven generations of bacterial replication at 6 hpi (Fig. 1B). Our infection screening parameters therefore allow identification of mutations that impair replication in this host, as well as mutations that cause sensitivity to killing by *G. mellonella* immune system components.

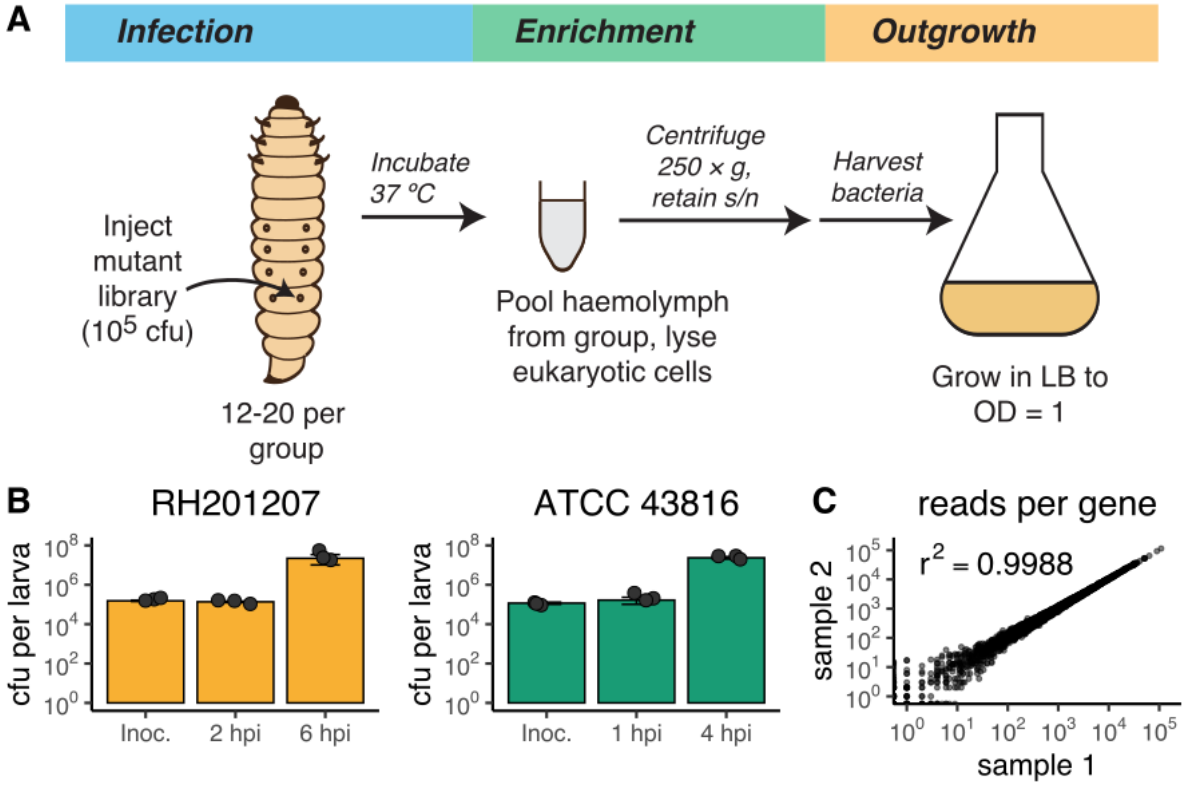

225

226 **Figure 1: Overview of transposon insertion screening in *Galleria mellonella* larvae** A:
227 Schematic of experimental procedure. Groups of larvae were injected with a pooled library of
228 *Klebsiella pneumoniae* transposon mutants and incubated at 37 °C for up to 6 hours.
229 Haemolymph was extracted from infected larvae, pooled and treated to remove eukaryotic
230 cells. Surviving bacteria were then grown in LB to generate sufficient material for sequencing.
231 B: Per-larva bacterial counts over the course of *G. mellonella infection*. Bacteria were
232 recovered when the load per larva reached approximately 10 million colony forming units
233 (cfu). The experiment was done in triplicates, closed circles represent one measurement, error
234 bars denote standard deviation. Abbreviation: Inoc., inoculum. C: Reads per gene of two
235 biological replicates of the unchallenged RH201207 input transposon library and their Pearson
236 correlation coefficient.

237

238 *Re-sequencing of RH201207*

239 During the initial analysis of the TraDIS experiments, we identified a possible mis-assembly
240 of the original RH201207 genome, which could not be improved by optimising the assembly
241 parameters. To improve the assembly and generate a circularised chromosome sequence, we
242 sequenced RH201207 by long-read Oxford Nanopore Technologies (ONT) sequencing.

Nanopore GridION sequencing yielded 2.3 G bases with an average read length of 10.5 kb and maximum read length of 165.9 kb, corresponding to ~400-fold theoretical coverage. Hybrid assembly of these reads together with existing MiSeq reads from Jana *et al* (1.24 million reads, ~35-fold genome coverage) yielded a circularised chromosome of 5,475,789 bp and three circularised potential plasmids (Table 1) of 113,640 bp (contig RH201207_2, IncFIB(pQil) and IncFII(K) replicons), 43,380 bp (contig RH201207_5, IncX3 replicon) and 13,841 bp length (contig RH201207_8, ColRNAI replicon). The remaining contigs of 202,245 bp length could not unambiguously be closed and circularised due to the presence of potential duplicated sequences. Nonetheless, typical plasmid replication proteins and the two replicons IncFIB(K) and IncFII(K) were present on these contigs, indicating that they are likely to be derived from plasmids (Table 1 and Fig. S1). The re-annotated RH201207 genome has 5,787 genes in total (5,546 protein-coding). and encodes a capsule of type KL106 and an O-antigen of type O2v2 as determined by Kaptive (Wick *et al.* 2018).

Identification of infection-related genes

TraDIS sequencing, read mapping and quantification of each transposon insertion site was performed using the Bio::TraDIS pipeline (Barquist *et al.* 2016). Each sample yielded from 12.9 million to 15.1 million transposon-tagged reads, > 89 % of which unambiguously mapped to the RH201207 chromosome (excluding unscaffolded contigs and plasmids) (Table S2). Analysis of the unchallenged RH201207 TraDIS library showed a total of more than 500,100 unique transposon insertion sites distributed across the chromosome, which corresponds to one insertion in every eleven nucleotides (Table 2). 638 genes (or 11.84 % of the 5390 chromosomal genes) were either essential or ambiguous-essential as defined by the Bio::TraDIS pipeline (Barquist *et al.* 2016), which is in good concordance with the first description of this library (Jana *et al.* 2017). A challenge in applying highly saturated transposon insertion libraries to infection models is the occurrence of bottlenecks, that is a stochastic drastic reduction in population size, which results in reduced genetic diversity of the population (Cain *et al.* 2020). We found a slight reduction in the diversity of the mutant library post-infection, with recovered unique insertion sites of nearly 380,000 and 360,000 total insertions (of 500,100) at 2 hpi and 6 hpi, respectively, however transposon insertion density remained very high with an insertion approximately every 15 bp (Table 2). To test if the loss of mutant library diversity had compromised the resolution of our experiment, we compared individual replicates using linear correlation analyses. Pearson correlation coefficients between *in vivo* replicates were very high with r^2 values greater than 0.98 when

analysing reads per gene and insertion indices per gene, and 0.69 to 0.77 when analysing the reads per unique insertion site (Fig. 1, S2, S3 and Table S3). Therefore, although our TraDIS experiments show a mild bottleneck, this is highly unlikely to affect any downstream analyses that use gene-level metrics. To identify *in vivo* fitness genes, the numbers of transposon insertion reads within each gene were compared between the *Galleria* infection and the inoculum pools, with essential and ambiguous-essential genes excluded to reduce false positives. Our analysis identified mutants of 133 (of 4,752) nonessential genes to be significantly less abundant at 6 hpi and two features, *rseA* and KPNRH_05271 to be slightly, but significantly enriched (Fig. 2 and supplementary table S4). 35 genes were so severely depleted after infection that they can be considered conditionally essential in *G. mellonella* (Table S4).

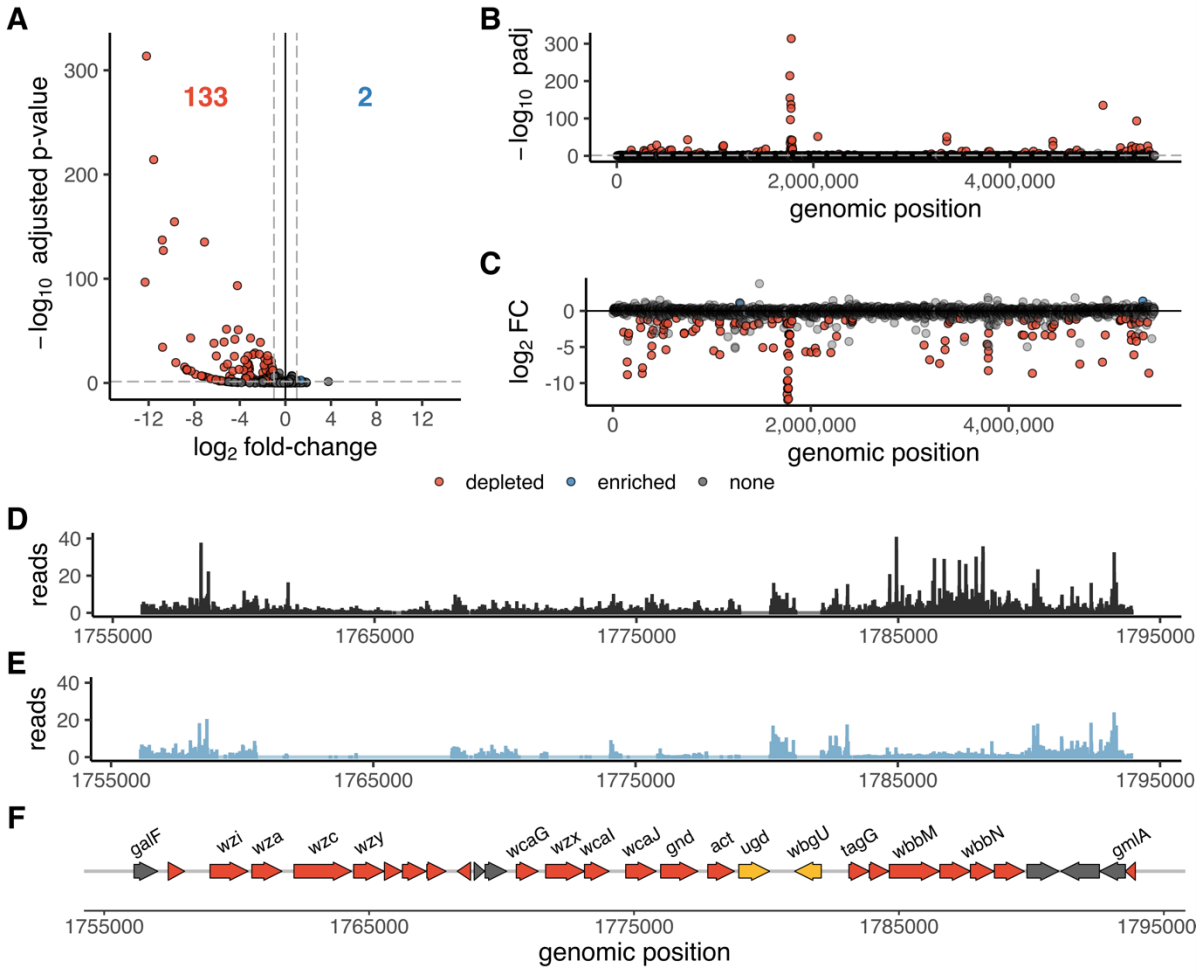

Figure 2: TraDIS analysis identifies multiple potential *K. pneumoniae* fitness factors important during *G. mellonella* infections. A: Volcano plot showing significantly less abundant genes 6 h after infecting *G. mellonella* larvae in red and significantly higher abundant genes in blue. Non-significant genes are shown in grey. Genes were considered significant if

they possessed a Benjamini-Hochberg corrected *p*-value below a threshold of 0.05 and an absolute log2 fold-change greater than 1. Essential and ambiguous-essential genes are removed from the analysis. B and C: Manhattan plots with Benjamini-Hochberg corrected *p*-value and log2 fold-change on the y-axis, respectively. Abbreviations: padj, Benjamini-Hochberg corrected *p*-value; FC, fold-change. D and E: Reads per nucleotide of the inoculum and at 6 hpi, respectively of the chromosomal region containing the K- and O-locus. For this graphical representation, triplicate TraDIS samples were combined and reads were normalised to the total number of reads in all three replicates. F: Gene annotations of the *Klebsiella* K-locus (*galF* to *wbgU*) and O-locus (*tagG* to *gmlA*), encoding the polysaccharide capsule and lipopolysaccharide O antigen, respectively are coloured according to the TraDIS results at 6 h post-infection; significantly depleted genes are shown in red, essential genes which were not included in the analysis in yellow and genes without significant changes in grey.

Surface polysaccharides, cell envelope and iron acquisition genes are critical to c*Kp* ***G. mellonella*** infection

Capsule, lipopolysaccharide and enterobacterial common antigen

Capsule and lipopolysaccharide (LPS) are essential to the virulence of *K. pneumoniae,* (Podschun and Ullmann 1998). The capsule allows *K. pneumoniae* to circumvent host detection and prevent an early immune response; acapsular mutants are less virulent in mouse models and are unable to spread systemically (Paczosa and Mecsas 2016). The lipopolysaccharide, consisting of lipid A, core and O antigen is able to bind and sequester parts of the complement system (Paczosa and Mecsas 2016). Both surface polysaccharides also play a role in modulating innate immunity (Bengoechea and Sa Pessoa 2019). Following *G. mellonella* infection, the eight genes with the most dramatic reduction in read counts (log2 fold-change < -12) all belonged to the capsule or O-antigen loci (Fig. 2B & C), and almost all genes in these clusters were significantly depleted (Fig. 2D-F).

Four genes (*wzxE*, *wecD*, *rffH*, *wecA*) of the Enterobacterial common antigen (ECA) synthesis locus (encoded by genes *rho*/KPNRH_05213 to yifK/KPNRH_05200) were also significantly depleted at 6 hpi (Fig. 2B & C). The ECA is a conserved carbohydrate antigen common to most Enterobacterales and plays an important role in bacterial physiology and its interaction with the environment (Rai and Mitchell 2020). *K. pneumoniae* ECA synthesis mutants were attenuated in *in vitro* murine lung and spleen tissues infections, but not *in vivo*

in a murine intranasal infection model (Lawlor *et al.* 2005). Therefore, our analysis identified mutants of all three major polysaccharide antigens (O, K and ECA) present on the cell surface (Rai and Mitchell 2020) to be attenuated in *G. mellonella*.

Cell envelope proteins and regulators

Genes that encode cell envelope proteins appeared to be important during *G. mellonella* infection. The major outer membrane lipoprotein Lpp (also known as Braun's lipoprotein) encoded by *lpp*/KPNRH_02211, and the genes of the Tol-Pal system (*pal*/KPNRH_03757, *tolB*/KPNRH_03758, *tolA*/KPNRH_03759 and tolQ/KPNRH_03761) (located at 3.8 Mbp) were significantly depleted after 6 hpi. The Tol-Pal system is involved in maintaining outer membrane integrity and consists of five proteins: TolA, TolQ, and TolR in the inner membrane, TolB in the periplasm, and the peptidoglycan-associated lipoprotein Pal anchored to the outer membrane (Lloubès *et al.* 2001). Lpp is a crucial protein in the outer membrane covalently linking it with the peptidoglycan layer (Asmar and Collet 2018) and it is important for complement resistance in multiple, phylogenetically distinct *K. pneumoniae* strains (Short *et al.* 2020). Mutations in both Lpp and Tol–Pal have been previously linked to attenuated virulence in diverse bacteria (Sha *et al.* 2008; Godlewska *et al.* 2009; Asmar and Collet 2018). One of the most abundant proteins in the outer membrane is the porin OmpK36 (Hernández-Allés *et al.* 1999) and mutants thereof were attenuated in a *G. mellonella* model (Insua et al. 2013) and a pneumonia mouse model (March et al. 2013). Likewise, our experiments identified a significant underrepresentation of transposon insertion mutants in *ompK36* (KPNRH_01613) 6 hours post-infection.

Also required for infection were regulators of cell envelope composition and integrity. Mutants of *phoPQ* were significantly less abundant following infection. PhoP-PhoQ is a two-component system, comprising the inner membrane sensor PhoQ and the cytoplasmic regulator PhoP. This system regulates lipid A remodelling in *K. pneumoniae in vivo* and *in vitro* (Llobet *et al.* 2015) and other virulence-associated genes in many enteric pathogens (Groisman 2001; Bijlsma and Groisman 2005; Alteri *et al.* 2011; Lin *et al.* 2018). *Salmonella* Typhimurium knockout strains of *phoP* and *phoQ* are highly attenuated for virulence in macrophages and a mouse infection (Miller, Kukral and Mekalanos 1989) and this two-component system also makes a small contribution to *K. pneumoniae* virulence during *G. mellonella* infections (Insua *et al.* 2013). We also noted significant changes in mutant abundance of genes related to the alternative sigma-factor RpoE (σ^{24} or σ^{E}), one of the major

regulators of cell envelope stress response systems (Flores-Kim and Darwin 2015; Roncarati and Scarlato 2017) (Treviño-Quintanilla, Freyre-González and Martínez-Flores 2013). RpoE activity is tightly controlled by a proteolytic cascade: after dissociation of RseB from RseA (the anti-sigma factor which binds RpoE), RseA is partially cleaved by the proteases DegS and RseP, then fully degraded by other cellular proteases such as ClpP/X-A, Lon and HslUV, releasing RpoE in the cytoplasm (Roncarati and Scarlato 2017). While *rpoE* itself and *rseP* are essential genes and therefore not included in our analysis, transposon insertion mutants of *degS*, *clpP*, *clpX* and *lon* were significantly less abundant, highlighting the role of RpoE gene regulation during infection. Transposon mutants of the RpoE inhibitor RseA and insertions in the promoter of the RseA-degrading protease HslUV (KPNRH_05271) were enriched after infection, indicating that increased RpoE signalling can enhance fitness in *G. mellonella*. Both RseA and HslUV are, via RpoE, involved in stress response and the regulation of virulence genes in multiple Enterobacteriaceae species (Flores-Kim and Darwin 2015). Interestingly, none of the RpoE regulated cell envelope stress response systems CpxAR, BaeRS, Rcs, and Psp (Flores-Kim and Darwin 2015) were identified in our screen, indicating either a redundancy in these systems or the involvement of other factors. Such factors could be the periplasmic chaperones Skp and SurA; both are members of the RpoE regulon in *E. coli* (Dartigalongue, Missiakas and Raina 2001). Mutants of *skp* and *surA* were less abundant in *Galleria* TraDIS and have previously been shown to be involved in pathogenicity in *E. coli*, *Salmonella* Typhimurium, *Shigella flexneri* and *Pseudomonas aeruginosa* (Sydenham *et al.* 2000; Redford and Welch 2006; Purdy, Fisher and Payne 2007; Klein *et al.* 2019).

Iron acquisition systems

Iron acquisition is essential during *K. pneumoniae* infections, and RH201207 produces the siderophores enterobactin and yersiniabactin to chelate host iron. Because siderophores confer benefits to bacterial populations, rather than individual cells, loss of siderophore biosynthesis genes is not expected to influence fitness in a mutant pool, and siderophore synthesis genes were not identified by the *Galleria* infection TraDIS. Utilisation of enterobactin was, however, important: mutations in three of the four ferric iron-enterobactin uptake complex components *tonB* (KPNRH_02155), *exbB* (KPNRH_00722), and *exbD* (KPNRH_00723) reduced fitness in *G. mellonella*. TonB is essential for pathogenicity in multiple bacteria, including hypervirulent *K. pneumoniae* (Hsieh *et al.* 2008). The fourth component of this complex, *fepB*, was present in multiple copies in the RH201207 genome,

so presumably mutation of just one gene does not cause loss of function. Mutation of the yersiniabactin receptor gene *fyuA* did not impair fitness, suggesting that enterobactin is sufficient to allow bacterial replication in the *G. mellonella* haemolymph. This is consistent with the roles of *K. pneumoniae* siderophores in murine infections, where enterobactin alone allows replication in serum by sequestering iron from transferrin (Bachman *et al.* 2012). Transferrin is also present in the haemolymph of *G. mellonella* (Vogel *et al.* 2011).

Further genes involved in Galleria mellonella *fitness*

Additional metabolic and hypothetical genes also contributed to fitness during *Galleria* infection. These included the majority of genes in the *aro* operon for synthesis of chorismite (a precursor to aromatic amino acids), *cys* genes for sulphate assimilation and cysteine biosynthesis, purine biosynthesis genes, several components of the electron transport complex, and *sspAB* stringent response proteins. Only 11 genes of unknown function were identified as infection-related (note some K- and O-locus genes were initially annotated as hypothetical). Several transcription regulators were also identified that compromised fitness when mutated: these were the arginine/lysine synthesis repressor *argP*, the fatty acid regulator *fabR*, the zinc-dependent repressor *nrdR* and the nickel-dependent repressor *yqjI*.

Temporal analysis of the *K. pneumoniae* RH201207 *G. mellonella* infection

We also analysed bacteria at 2 hpi, in order to gain insight into the events of early infection, and distinguish mutations influencing survival in the presence of *G. mellonella* immune system components from those influencing replication in this host. Mutants in 54 genes were significantly less abundant at 2 hpi, and only mutants lacking the cell division protein FtsB were enriched (Fig. 3, S4-S6 and supplementary table S4). Comparison of both timepoints showed 18 genes depleted only at 2 hpi, 36 genes less abundant at both timepoints and 97 genes for which mutant abundance was reduced only at 6 h post-infection (Fig. 3A). The genes that were depleted at both time points consists of two subsets: 25 genes that are depleted within the first 2 h and whose abundance does not change further, and 11 genes that are depleted at 2 hpi and then further decrease in abundance over time. Ten out of these 11 genes are part of the K-locus, the other one is *tagG*, the first gene of the neighbouring O antigen locus.

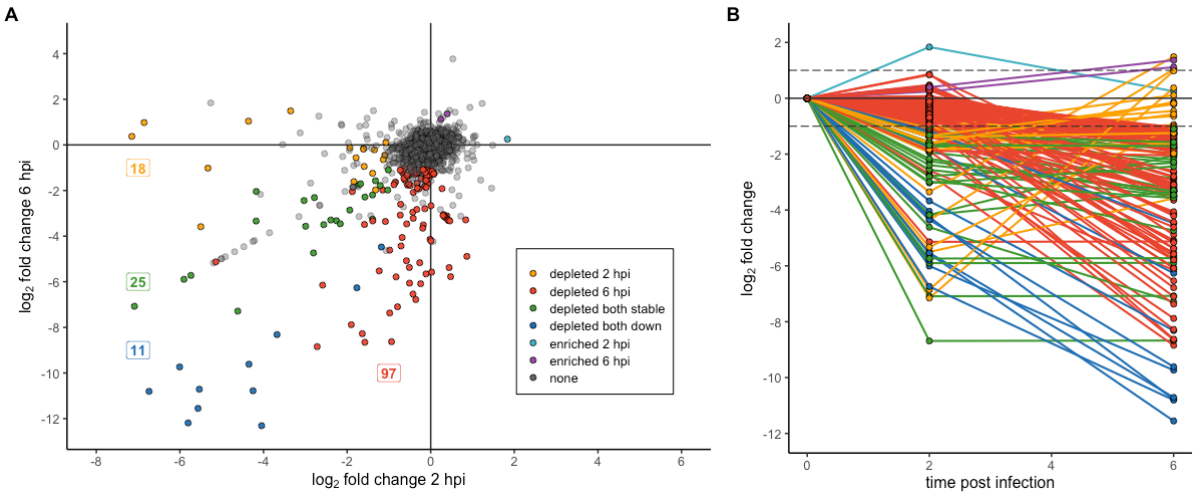

Figure 3: Few genes are important for the onset but not the late stages of a *G. mellonella* infection. A: The plot shows log2 fold-changes at 2 hpi and 6 hpi on the x- and y-axis, respectively. Transposon mutants significantly less abundant at 2 hpi and 6 hpi are shown in yellow and red, respectively. Mutants which are depleted at both timepoints are shown in either green or blue (if the log2 fold-change at 2 hpi roughly equals that at 6 hpi in green and if their abundance was much lower at 6 hpi in blue). Genes significantly higher abundant at 2 hpi and 6 hpi are shown in turquois and purple, respectively. Non-significant genes are shown in grey. Numbers indicate the number of genes of each group. B: Graph highlighting the direction of the log2 fold-change change over time. Genes are coloured according to A; non-significant genes are not shown.

Of the 18 genes less abundant only at the beginning of the infection, most were barely within our threshold for fitness-related genes. But six genes had log2 fold-changes of -3 up to -7, among them two tRNAs, one hypothetical protein and the three genes *oxyR* (KPNRH_05248), *rnhA* (KPNRH_04380) and *tadA* (KPNRH_01302). It is very likely that the tRNAs are false positives due to their very short length and therefore low number of insertions. OxyR is a conserved LysR-type transcription factor which plays a key role in the regulation of defence mechanisms against oxidative stress (Christman, Storz and Ames 1989), and has previously been linked to *K. pneumoniae* pathogenesis (Hennequin and Forestier 2009). RnhA is the ribonuclease HI that cleaves RNA of RNA–DNA hybrids and is involved in DNA replication, DNA repair, and RNA transcription (Kochiwa, Tomita and Kanai 2007) and *tadA* encodes a tRNA-specific adenosine deaminase. This protein is

441 responsible for adenosine to inosine RNA editing of tRNAs and mRNAs, and is involved in
442 the regulation of a toxin-antitoxin system in *E. coli* (Bar-Yaacov *et al.* 2017).

443 Of all significantly less abundant insertion mutants, the by far largest set, consisting of 97
444 genes, is depleted only at the later timepoint 6 h after infection. This group of genes contains
445 for example the two-component system *phoPQ,* the Tol–Pal system and the majority of genes
446 of the O antigen cluster. Our data indicates that these genes might only have a minor impact
447 on fitness during very early stages of infection.

448 **Shared *in vivo* fitness determinants in c*Kp* RH201207 and hv*Kp* ATCC 43816**

449 We then sought to compare the *G. mellonella* fitness landscape of the c*Kp* ST258 strain
450 RH201207 with a representative hv*Kp* strain. *G. mellonella* infection TraDIS was performed
451 with the well-studied mouse-virulent strain ATCC 43816, which is an ST493 strain
452 possessing type O1v1 O antigen and K2 capsule type. Experiments were performed in the
453 same way as for RH201207 except that bacteria were recovered for sequencing at 4 hpi, due
454 to the faster progression of infection when using this strain (Fig. 1B). Each sample of ATCC
455 43816 yielded from 1.85 million to 2.08 million reads, more than 96 % of which were
456 reliably mapped to the chromosome of ATCC 43816 KPPR1 (CP009208.1) (Table S2). The
457 insertion density of the unchallenged ATCC 43816 mutant library was 415,000 or one
458 insertion per 13 nucleotides, which is similar to the RH201207 library (Table 2, S2), and 502
459 genes were classified as essential or ambiguous-essential (9.62 % of 5217 genes).
460 Reproducibility between experimental replicates was very high in this experiment, with
461 Pearson correlation coefficient > 0.97 for reads or insertion indices per gene, and > 0.91
462 when comparing reads per unique insertion site (Fig. S2, S3 and Table S3).

463 We identified 92 nonessential genes of *K. pneumoniae* ATCC 43816 that had significantly
464 lower mutant abundance after the *Galleria* infection and two genes (VK055_RS06420 and
465 VK055_RS19345) that were enriched (Fig. S4-S6 and supplementary table S5). Mutants in
466 10 genes of the 18-gene K locus of ATCC 43816 were significantly depleted after
467 *G. mellonella* infection, thereby mirroring the results of RH201207. In contrast, genes of the
468 O-locus were not implicated in *in vivo* fitness in *G. mellonella*. This was unexpected because
469 our previous study showed that O antigen genes were required for ATCC 43816 serum
470 resistance (Short *et al.* 2020) and we predicted that resistance to *G. mellonella* humoral
471 immunity may have similar requirements. However other studies of ATCC 43816 O antigen
472 have shown variable effects on virulence and related *in vitro* phenotypes (Shankar-Sinha *et*

al. 2004; Yeh *et al.* 2016). We speculate that the ATCC 43816 capsule has a dominant role in protection from *G. mellonella* immunity and masks the activity of O antigen.

To compare the global TraDIS results from RH21207 with those of ATCC 43816, we identified their shared genes by bidirectional best hits BLAST search using a sequence similarity cut-off of 80 %. This analysis identified 4,391 shared genes, 3,974 of which were non-essential in both strains and therefore included in the comparison. We identified 149 shared genes with a role in *G. mellonella* infection in either RH201207 or ATCC 43816, and 44 genes were implicated in both strains (Fig. 4A). This means that 37.3 % of the hits in RH201207 were also identified in ATCC 43816 and 58.7 % of all hits in ATCC 43816 were identified in either of the two RH201207 datasets, the largest overlap was with the later timepoint of 6 hpi. Amongst those genes were, for example, the membrane-associated genes *ompK36, tolABQ, and lpp,* the outer membrane protein assembly factor *bamB/yfgL,* the periplasmic chaperone *surA,* and the ECA synthesis genes *rffG* and *wecA.*

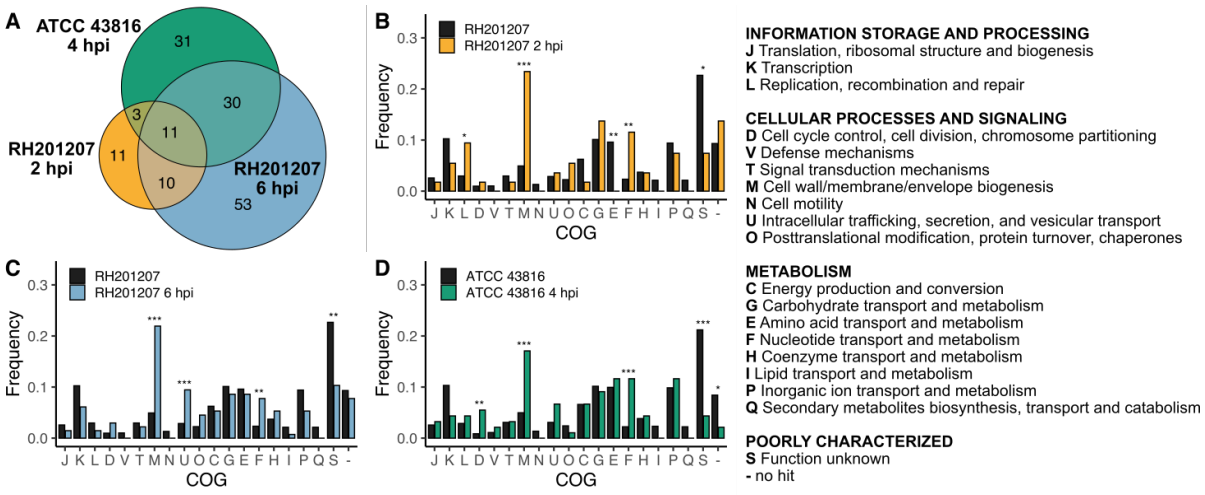

Figure 4: Multiple genes, including the cps cluster contribute to the fitness during *Galleria* infections of both classical and hypervirulent *K. pneumoniae*. A: Venn diagram showing the overlap of significantly less abundant insertion mutants in the classical ST258 strain RH201207 and the hypervirulent strain ATCC 43816. Only non-essential genes shared by both strains as determined by a bi-directional best blast analysis are shown. B-D: Cluster of orthologous groups (COG) enrichment analysis shows an overrepresentation of outer membrane biogenesis as well as nucleotide transport and metabolism genes in all sets of significantly depleted genes during *G. mellonella* infection. Genes were assigned to Cluster of Orthologous Groups (COG) (Tatusov *et al.* 2000) with eggNOG. The bars represent the percentage of genes that belong in that category. Black bars denote the frequency of COGs in

all non-essential genes of the particular strain, the frequency of all significantly depleted genes after *Galleria* infection is coloured as follows, A: RH201207 2 hpi, B: RH201207 6 hpi, C ATCC 43816 4 hpi. *P*-values were determined by Fisher's exact test in R and the level of significance is indicated by asterisks (*, $P < 0.05$; **, $P < 0.01$; ***, $P < 0.001$). COGs without genes assigned to them (A, B, R, W, Y & Z) were removed.

We performed a clusters of orthologous groups (COG) enrichment analysis to define and compare the broad pathways and molecular mechanisms that may contribute to fitness during *G. mellonella* infections in both strains. The COG classifications of the genes in the RH201207 and the ATCC 43816 genome was annotated with EggNOG Mapper (Huerta-Cepas *et al.* 2017) and the COGs of all genes in which mutants were significantly underrepresented after infection were compared to the total gene set. In RH201207, genes of the replication, recombination and repair (L), cell wall/membrane/envelope metabolism (M) and nucleotide transport and metabolism (F) clusters were overrepresented among the infection-related genes at 2 hpi, whereas amino acid transport and metabolism (E) and genes of unknown function (S) were underrepresented (Fig. 4B). At 6 h post-infection, cell wall/membrane/envelope metabolism (M), intracellular trafficking, secretion, and vesicular transport (U) and nucleotide transport and metabolism (F) were overrepresented, whereas only genes of unknown function (S) were underrepresented (Fig. 4C). In the ATCC 43816 infection determinants, genes assigned to carbohydrate transport and metabolism (G), cell wall/membrane/envelope biogenesis (M) and nucleotide transport and metabolism (F) were overrepresented. The cell wall/membrane/envelope metabolism (M) and nucleotide transport and metabolism (F) clusters were the only ones in which infection-related genes were overrepresented for both c*Kp* and hv*Kp*, and at early and late time points. This finding further stresses the importance of cell membrane integrity and surface polysaccharides in infections, but also demonstrates the essentiality of nucleotide metabolism during the course of an infection. The latter COG included the genes *purA*, *purC*, *purE*, *purH*, and *rdgB*; all purine biosynthesis genes that showed significantly reduced fitness in both strains. The ability to *de novo* synthesize purines has been associated with the intracellular survival of bacterial pathogens such as *Burkholderia pseudomallei, Shigella flexneri, and* uropathogenic *Escherichia coli* (Ray *et al.* 2009; Shaffer *et al.* 2017).

Comparison with genetic fitness requirements in murine hosts and *in vitro* virulence screens

We then sought to compare our findings in *G. mellonella* to published results of other high-throughput fitness screens of *K. pneumoniae*, with the caveat that such screens by their nature provide only a snapshot of the events of an infection, and are unlikely to be comprehensive.

The *G. mellonella* fitness genes identified in both strains showed considerable similarity to those required for survival in human serum, which we examined previously using the same mutant libraries (Short *et al.* 2020). This was largely due to the importance of capsule, O antigen and cell envelope proteins such as Lpp for survival under both selections; the many metabolic genes identified as infection-relevant, for example those of purine biosynthesis (Fig. 4), generally did not contribute to serum survival. For RH201207, over half of the genes identified as required for full serum fitness also contributed to fitness in *G. mellonella*.

Fitness factors required for intestinal colonisation of mice have also been examined in an ST258 background (Benoit *et al.* 2019), although this screen was not comprehensive due to various experimental factors. Several genes required in *G. mellonella* are also required for intestinal colonisation, such as *bamB* (an outer membrane assembly protein), *ompC/ompK36*, *cyaA*, (adenylate cyclase) and *typA* (a GTP-binding protein). Finally, there are some important common factors among the requirements for infection of *G. mellonella*, and for an hv*Kp* murine lung infection (Paczosa *et al.* 2020). Genes contributing to both infection types include some of those encoding ubiquitous virulence factors such as capsule or siderophore importers. Notably, genes involved in aromatic amino acid biosynthesis (e.g. *pabAB* aminodeoxychorismate synthase, *aro* operon genes), and purine biosynthesis (e.g. *purH*) were required both for murine lung infection, and for *Galleria mellonella* infection in both strain backgrounds. The importance of these pathways for two very different types of infection, in representatives of both hv*Kp* and c*Kp*, suggests that they may be general infection requirements for *K. pneumoniae*.

Validation of transposon insertion sequencing results and investigation of NfeR activity

Five single-gene mutants of *K. pneumoniae* RH201207 were tested for lethality in *G. mellonella* to validate the TraDIS screen. The validation set included transposon insertion mutants in the transcription antiterminator *rfaH*, the capsule gene *wzc* and the enterobacterial common antigen gene *wzxE*, as well as clean deletion mutants of *phoQ* and *nfeR*. Research-grade *G. mellonella* larvae were injected with 10^6 cfu of each strain, or a PBS control, and

monitored for up to 72 hours. All strains showed a statistically significant virulence defect (Fig. 5A), with the exception of RH201207 Δ*phoQ*; larvae infected with the Δ*phoQ* mutant showed increased survival but the degree did not reach statistical significance. It is possible that the TraDIS screen detected changes that reflect fitness in a competition environment with other strains, or that are important at early stages of infection but are not relevant in the longer term.

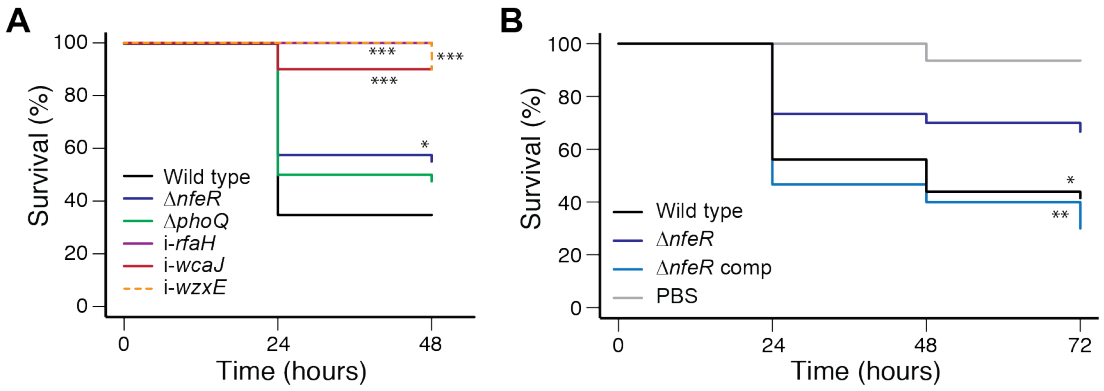

Figure 5: Validation of TraDIS results with single-gene knockouts. A: Survival curves for *G. mellonella* larvae following infection with *K. pneumoniae* RH201207 and mutants in defined genes. B: Complementation of the virulence defect of RH201207 Δ*nfeR*. Mutants where survival is significantly different to wild-type (Kaplan-Meier test) are indicated by asterisks (*, P <0.05; **, $P < 0.01$; ***, $P < 0.001$).

We selected *nfeR* (KPNRH_00645 also called *yqjI*) for further characterisation, as this gene has not previously been linked to virulence in any species. In our TraDIS experiments, this gene was required in *K. pneumoniae* RH201207, but not in ATCC 43816. Complementation of the Δ*nfeR* mutation restored the virulence of the wild-type RH201207 strain (Fig. 5B). NfeR contributes to metal homeostasis in *E. coli* by repressing expression of a neighbouring ferric reductase gene, *nfeF* (Fig. 6A); this repression is relieved under excess nickel conditions (Wang, Wu and Outten 2011; Wang *et al.* 2014). High nickel levels can disrupt iron homeostasis in *E. coli*, leading to a longer lag phase due to reduced accumulation of iron (Rolfe *et al.* 2012; Washington-Hughes *et al.* 2019). We hypothesised that loss of *nfeR* may lead to deregulated metal homeostasis in *K. pneumoniae* RH201207, resulting in reduced virulence in *Galleria mellonella*.

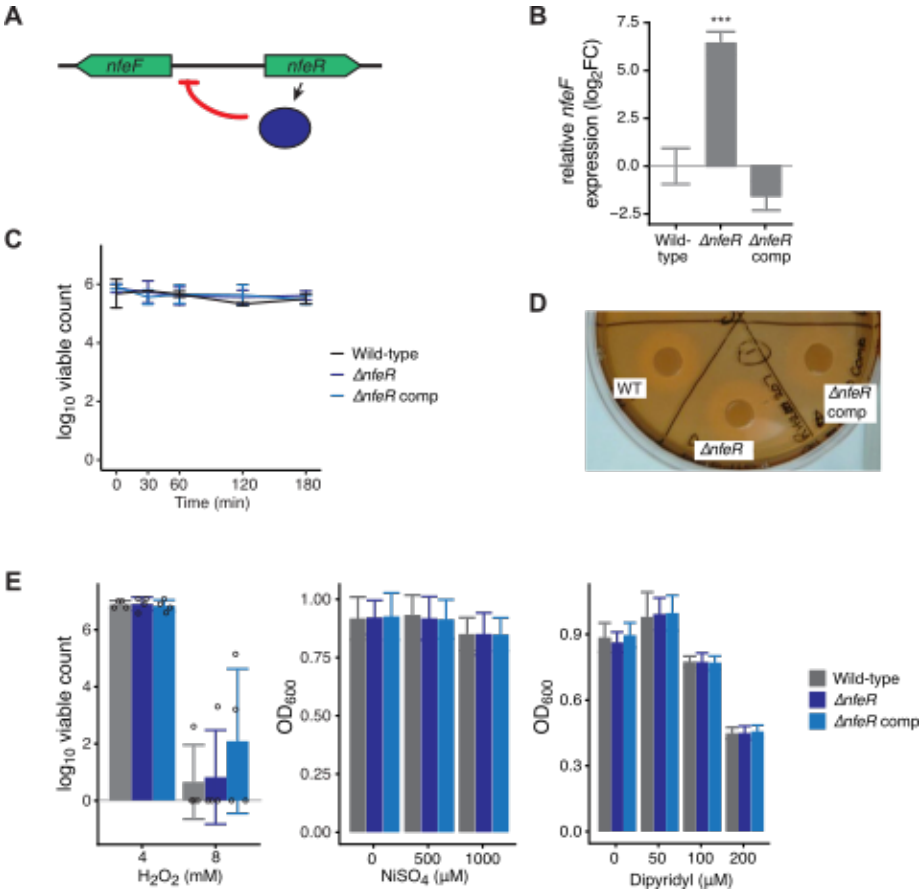

584

585 **Figure 6: Investigation of NfeR function in RH201207.** Mutation of *nfeR* resulted in a
586 dramatic increase in *nfeF* expression. A: Schematic of *nfeF* gene expression regulation by
587 NfeR. B: Deletion of *nfeR* leads to significant overexpression of *nfeF* as measured by qRT-
588 PCR. Level of significance in comparison to RH201207 is indicated by asterisks (***, $P <$
589 0.001). C: Serum survival of RH201207 Δ*nfeR*. Late exponential phase bacteria were incubated
590 in 66 % normal human serum for 3 hours, and viable counts measured over time. D:
591 Siderophore production by RH201207 Δ*nfeR*, using chrome azurol S agar assay. Results shown
592 are representative of two independent experiments, each comprising at least two biological
593 replicates. E: Sensitivity of RH201207 Δ*nfeR* to hydrogen peroxide, Nickel toxicity and
594 dipyridyl-induced metal starvation. Stationary phase cells were diluted directly into H_2O_2-
595 supplemented Mueller Hinton broth, and surviving cells enumerated after 100 min. For Nickel
596 and dipyridyl toxicity, growth was measured after incubation for 18 hours at 37 °C. Results
597 shown are the mean and standard deviation of four (H_2O_2) or three biological replicates, which
598 in the case of Ni and dipyridyl comprised of 3 technical replicates.

599

We first tested whether NfeR regulates *nfeF* expression in *K. pneumoniae* RH201207 by qRT-PCR using RNA extracted from late exponential phase bacteria. As shown (Fig. 6B), deletion of *nfeR* caused a dramatic 85-fold increase in *nfeF* expression, and this change was not seen in the complemented strain. We hypothesised that the virulence defect of RH201207 Δ*nfeR* may arise from a reduced defence against humoral immunity, or reduced ability to acquire iron, as *G. mellonella* recapitulates several relevant features of mammalian serum-based immunity, and is iron-limited (Lucidi *et al.* 2019). However, the mutant did not show any differences relative to its wild type either in its ability to withstand serum exposure (Fig. 6C), or its siderophore production (Fig. 6D). Finally, we examined three phenotypes that may be disrupted when metal homeostasis is altered: resistance to oxidative stress (hydrogen peroxide), nickel toxicity and sensitivity to iron starvation. Sensitivity to oxidative stress is influenced by cellular iron pools, and was previously shown to be growth-phase dependent for this reason (Touati 2000). Homologues of *nfeR* have been implicated in resistance to nickel toxicity in large-scale fitness screens (Price *et al.* 2018). It was also shown that some genes in the same pathway as *nfeF* are more sensitive to dipyridyl-mediated iron starvation (McHugh *et al.* 2003). However, *K. pneumoniae* RH201207 Δ*nfeR* did not show changes in any of these phenotypes. Thus, while Δ*nfeR* mutation increases *nfeF* expression and reduces virulence, its mechanism appears to be via subtle effects that are not replicated *in vitro*.

Conclusions

Despite the urgency of the public health threat posed by classical, multidrug-resistant *K. pneumoniae* strains, our understanding of their mechanisms of infection are still limited. *Galleria mellonella* is an increasingly popular alternative model for bacterial infections, which, unlike mice, is susceptible to infection by c*Kp*. Here, we have performed the first high-throughput fitness profiling study of *K. pneumoniae* during *G. mellonella* infection.

G. mellonella had favourable infection parameters for high-throughput screening; the diversity of the highly saturated transposon mutant library was largely maintained through the experiment, and excellent reproducibility was achieved between biological replicates. Infection-related genes identified showed high concordance with current knowledge of *K. pneumoniae* pathogenesis; all of the major virulence factors (siderophores, capsule, O antigen) showed decreased mutant abundance, and many new virulence gene candidates were identified in c*Kp*. This included the metal-dependent regulator *nfeR*, which did not

contribute to virulence in the hv*Kp* background. A limitation of our study, and indeed the majority of studies providing molecular detail on *G. mellonella*-pathogen interactions, is that these putative virulence factors have not been further examined in mammalian models.

Our results showed a substantially different fitness landscape for RH201207 and ATCC43816 during *G. mellonella* infection. Fewer infection-related genes were identified in *K. pneumoniae* ATCC43816 (hv*Kp*). This finding may reflect masking of some relevant activities by dominant virulence factors; for example, the highly expressed K2 capsule of this strain may compensate for loss of other cell envelope components, such as multiple genes involved in RpoE signalling which were required in the c*Kp* background. The complex interplay of virulence factors underscores the need to consider the phylogenetic diversity of *K. pneumoniae* when studying its pathogenesis.

We have demonstrated a simple, scalable method for virulence factor profiling in c*Kp*, and used it to provide the first genome-scale view of a c*Kp* infection and compare it to an hv*Kp* strain. The capacity of the *G. mellonella* model to elucidate relevant virulence activities, and the ease with which it can be applied to new strains, opens the possibility for robust species-wide comparisons of infection determinants in *K. pneumoniae* and other opportunistic pathogens.

Funding

This work was supported by a Sir Henry Wellcome postdoctoral fellowship to F.L.S. (grant 106063/A/14/Z) and by the Wellcome Sanger Institute (grant 206194).

Acknowledgements

We thank Matt Mayho, Kim Judge, and the sequencing teams at the Wellcome Sanger Institute for Nanopore and TraDIS sequencing, and the Pathogen Informatics team for support with bioinformatic analysis. We thank Luca Guardabassi and Bimal Jana for providing the RH201207 library.

References

Alteri CJ, Lindner JR, Reiss DJ *et al.* The broadly conserved regulator PhoP links pathogen virulence and membrane potential in Escherichia coli. *Molecular Microbiology* 2011;**82**:145–63.

661 Asmar AT, Collet J-F. Lpp, the Braun lipoprotein, turns 50—major achievements and
662 remaining issues. *FEMS Microbiol Lett* 2018;**365**, DOI: 10.1093/femsle/fny199.

663 Bachman MA, Lenio S, Schmidt L *et al.* Interaction of Lipocalin 2, Transferrin, and
664 Siderophores Determines the Replicative Niche of Klebsiella pneumoniae during
665 Pneumonia. *mBio* 2012;**3**, DOI: 10.1128/mBio.00224-11.

666 Barquist L, Mayho M, Cummins C *et al.* The TraDIS toolkit: sequencing and analysis for dense
667 transposon mutant libraries. *Bioinformatics* 2016;**32**:1109–11.

668 Bar-Yaacov D, Mordret E, Towers R *et al.* RNA editing in bacteria recodes multiple proteins
669 and regulates an evolutionarily conserved toxin-antitoxin system. *Genome Res*
670 2017;**27**:1696–703.

671 Bengoechea JA, Sa Pessoa J. Klebsiella pneumoniae infection biology: living to counteract
672 host defences. *FEMS Microbiology Reviews* 2019;**43**:123–44.

673 Benoit SL, Schmalstig AA, Glushka J *et al.* Nickel chelation therapy as an approach to combat
674 multi-drug resistant enteric pathogens. *Scientific Reports* 2019;**9**:13851.

675 Bijlsma JJE, Groisman EA. The PhoP/PhoQ system controls the intramacrophage type three
676 secretion system of Salmonella enterica. *Molecular Microbiology* 2005;**57**:85–96.

677 Cain AK, Barquist L, Goodman AL *et al.* A decade of advances in transposon-insertion
678 sequencing. *Nature Reviews Genetics* 2020;**21**:526–40.

679 Carattoli A, Zankari E, García-Fernández A *et al.* In Silico Detection and Typing of Plasmids
680 using PlasmidFinder and Plasmid Multilocus Sequence Typing. *Antimicrobial Agents*
681 *and Chemotherapy* 2014;**58**:3895–903.

682 Christman MF, Storz G, Ames BN. OxyR, a positive regulator of hydrogen peroxide-inducible
683 genes in Escherichia coli and Salmonella typhimurium, is homologous to a family of
684 bacterial regulatory proteins. *Proc Natl Acad Sci U S A* 1989;**86**:3484–8.

685 Dartigalongue C, Missiakas D, Raina S. Characterization of the Escherichia coli sigma E
686 regulon. *J Biol Chem* 2001;**276**:20866–75.

687 Diago-Navarro E, Motley MP, Ruiz-Peréz G *et al.* Novel, Broadly Reactive Anticapsular
688 Antibodies against Carbapenem-Resistant Klebsiella pneumoniae Protect from
689 Infection. *mBio* 2018;**9**, DOI: 10.1128/mBio.00091-18.

690 Dorman MJ, Feltwell T, Goulding DA *et al.* The Capsule Regulatory Network of Klebsiella
691 pneumoniae Defined by density-TraDISort. *mBio* 2018;**9**, DOI: 10.1128/mBio.01863-
692 18.

693 Dumigan A, Fitzgerald M, Santos JS-PG *et al.* A Porcine Ex Vivo Lung Perfusion Model To
694 Investigate Bacterial Pathogenesis. Allen IC, Goldberg JB (eds.). *mBio*
695 2019;**10**:e02802-19, /mbio/10/6/mBio.02802-19.atom.

696 Flores-Kim J, Darwin AJ. Regulation of bacterial virulence gene expression by cell envelope
697 stress responses. *Virulence* 2015;**5**:835–51.

698 Godlewska R, Wiśniewska K, Pietras Z *et al.* Peptidoglycan-associated lipoprotein (Pal) of
699 Gram-negative bacteria: function, structure, role in pathogenesis and potential
700 application in immunoprophylaxis. *FEMS Microbiol Lett* 2009;**298**:1–11.

701 Groisman EA. The Pleiotropic Two-Component Regulatory System PhoP-PhoQ. *Journal of*
702 *Bacteriology* 2001;**183**:1835–42.

703 Harding CR, Schroeder GN, Collins JW *et al.* Use of Galleria mellonella as a model organism
704 to study Legionella pneumophila infection. *J Vis Exp* 2013:e50964.

705 Hennequin C, Forestier C. oxyR, a LysR-Type Regulator Involved in Klebsiella pneumoniae
706 Mucosal and Abiotic Colonization. *Infection and Immunity* 2009;**77**:5449–57.

707 Hernández-Allés S, Albertí S, Álvarez D *et al.* Porin expression in clinical isolates of Klebsiella
708 pneumoniae. *Microbiology (Reading)* 1999;**145 (Pt 3)**:673–9.

709 Hsieh P-F, Lin T-L, Lee C-Z *et al.* Serum-Induced Iron-Acquisition Systems and TonB
710 Contribute to Virulence in Klebsiella pneumoniae Causing Primary Pyogenic Liver
711 Abscess. *J Infect Dis* 2008;**197**:1717–27.

712 Huerta-Cepas J, Forslund K, Coelho LP *et al.* Fast Genome-Wide Functional Annotation
713 through Orthology Assignment by eggNOG-Mapper. *Mol Biol Evol* 2017;**34**:2115–22.

714 Insua JL, Llobet E, Moranta D *et al.* Modeling Klebsiella pneumoniae Pathogenesis by
715 Infection of the Wax Moth Galleria mellonella. Bliska JB (ed.). *Infect Immun*
716 2013;**81**:3552–65.

717 Jana B, Cain AK, Doerrler WT *et al.* The secondary resistome of multidrug-resistant Klebsiella
718 pneumoniae. *Sci Rep* 2017;**7**:42483.

719 Kanehisa M, Goto S. KEGG: Kyoto Encyclopedia of Genes and Genomes. *Nucleic Acids Res*
720 2000;**28**:27–30.

721 Klein K, Sonnabend MS, Frank L *et al.* Deprivation of the Periplasmic Chaperone SurA
722 Reduces Virulence and Restores Antibiotic Susceptibility of Multidrug-Resistant
723 Pseudomonas aeruginosa. *Front Microbiol* 2019;**10**, DOI: 10.3389/fmicb.2019.00100.

724 Kochiwa H, Tomita M, Kanai A. Evolution of ribonuclease H genes in prokaryotes to avoid
725 inheritance of redundant genes. *BMC Evol Biol* 2007;**7**:128.

726 Langridge GC, Phan M-D, Turner DJ *et al.* Simultaneous assay of every Salmonella Typhi
727 gene using one million transposon mutants. *Genome Res* 2009;**19**:2308–16.

728 Lawlor MS, Hsu J, Rick PD *et al.* Identification of Klebsiella pneumoniae virulence
729 determinants using an intranasal infection model. *Molecular Microbiology*
730 2005;**58**:1054–73.

731 Li G, Shi J, Zhao Y *et al.* Identification of hypervirulent Klebsiella pneumoniae isolates using
732 the string test in combination with Galleria mellonella infectivity. *Eur J Clin Microbiol*
733 *Infect Dis* 2020;**39**:1673–9.

734 Lin Z, Cai X, Chen M *et al.* Virulence and Stress Responses of Shigella flexneri Regulated by
735 PhoP/PhoQ. *Front Microbiol* 2018;**8**, DOI: 10.3389/fmicb.2017.02689.

736 Llobet E, Martínez-Moliner V, Moranta D *et al.* Deciphering tissue-induced Klebsiella
737 pneumoniae lipid A structure. *PNAS* 2015;**112**:E6369–78.

738 Lloubès R, Cascales E, Walburger A *et al.* The Tol-Pal proteins of the Escherichia coli cell
739 envelope: an energized system required for outer membrane integrity? *Research in*
740 *Microbiology* 2001;**152**:523–9.

741 Louden BC, Haarmann D, Lynne AM. Use of Blue Agar CAS Assay for Siderophore
742 Detection. *J Microbiol Biol Educ* 2011;**12**:51–3.

743 Lucidi M, Visaggio D, Prencipe E *et al.* New Shuttle Vectors for Real-Time Gene Expression
744 Analysis in Multidrug-Resistant Acinetobacter Species: In Vitro and In Vivo
745 Responses to Environmental Stressors. *Appl Environ Microbiol* 2019;**85**, DOI:
746 10.1128/AEM.01334-19.

747 March C, Cano V, Moranta D *et al.* Role of Bacterial Surface Structures on the Interaction of
748 Klebsiella pneumoniae with Phagocytes. Forestier C (ed.). *PLoS ONE* 2013;**8**:e56847.

749 McHugh JP, Rodríguez-Quiñones F, Abdul-Tehrani H *et al.* Global Iron-dependent Gene
750 Regulation in *Escherichia coli*: A NEW MECHANISM FOR IRON HOMEOSTASIS.
751 *J Biol Chem* 2003;**278**:29478–86.

752 Miller SI, Kukral AM, Mekalanos JJ. A two-component regulatory system (phoP phoQ)
753 controls Salmonella typhimurium virulence. *PNAS* 1989;**86**:5054–8.

754 Paczosa MK, Mecsas J. Klebsiella pneumoniae: Going on the Offense with a Strong Defense.
755 *Microbiol Mol Biol Rev* 2016;**80**:629–61.

756 Paczosa MK, Silver RJ, McCabe AL *et al.* Transposon Mutagenesis Screen of Klebsiella
757 pneumoniae Identifies Multiple Genes Important for Resisting Antimicrobial Activities
758 of Neutrophils in Mice. *Infection and Immunity* 2020;**88**, DOI: 10.1128/IAI.00034-20.

759 Palacios M, Miner TA, Frederick DR *et al.* Identification of Two Regulators of Virulence That
760 Are Conserved in Klebsiella pneumoniae Classical and Hypervirulent Strains. *mBio*
761 2018;**9**, DOI: 10.1128/mBio.01443-18.

762 Pendleton JN, Gorman SP, Gilmore BF. Clinical relevance of the ESKAPE pathogens. *Expert*
763 *Review of Anti-infective Therapy* 2013;**11**:297–308.

764 Pereira MF, Rossi CC, da Silva GC *et al.* Galleria mellonella as an infection model: an in-depth
765 look at why it works and practical considerations for successful application. *Pathog Dis*
766 2020, DOI: 10.1093/femspd/ftaa056.

767 Podschun R, Ullmann U. Klebsiella spp. as Nosocomial Pathogens: Epidemiology, Taxonomy,
768 Typing Methods, and Pathogenicity Factors. *Clinical Microbiology Reviews*
769 1998;**11**:589–603.

770 Price MN, Wetmore KM, Waters RJ *et al.* Mutant phenotypes for thousands of bacterial genes
771 of unknown function. *Nature* 2018;**557**:503–9.

772 Purdy GE, Fisher CR, Payne SM. IcsA Surface Presentation in Shigella flexneri Requires the
773 Periplasmic Chaperones DegP, Skp, and SurA. *Journal of Bacteriology*
774 2007;**189**:5566–73.

775 R Core Team. R: A language and environment for statistical computing. 2019.

776 Rai AK, Mitchell AM. Enterobacterial Common Antigen: Synthesis and Function of an
777 Enigmatic Molecule. *mBio* 2020;**11**, DOI: 10.1128/mBio.01914-20.

778 Ray K, Marteyn B, Sansonetti PJ *et al.* Life on the inside: the intracellular lifestyle of cytosolic
779 bacteria. *Nature Reviews Microbiology* 2009;**7**:333–40.

780 Redford P, Welch RA. Role of Sigma E-Regulated Genes in Escherichia coli Uropathogenesis.
781 *Infect Immun* 2006;**74**:4030–8.

782 Rolfe MD, Rice CJ, Lucchini S *et al.* Lag phase is a distinct growth phase that prepares bacteria
783 for exponential growth and involves transient metal accumulation. *J Bacteriol*
784 2012;**194**:686–701.

785 Roncarati D, Scarlato V. Regulation of heat-shock genes in bacteria: from signal sensing to
786 gene expression output. *FEMS Microbiol Rev* 2017;**41**:549–74.

787 Russo TA, MacDonald U. The Galleria mellonella Infection Model Does Not Accurately
788 Differentiate between Hypervirulent and Classical Klebsiella pneumoniae. *mSphere*
789 2020;**5**, DOI: 10.1128/mSphere.00850-19.

790 Russo TA, Marr CM. Hypervirulent Klebsiella pneumoniae. *Clin Microbiol Rev* 2019;**32**, DOI:
791 10.1128/CMR.00001-19.

792 Schwyn B, Neilands JB. Universal chemical assay for the detection and determination of
793 siderophores. *Analytical Biochemistry* 1987;**160**:47–56.

794 Seemann T. Prokka: rapid prokaryotic genome annotation. *Bioinformatics* 2014;**30**:2068–9.

795 Sha J, Agar SL, Baze WB *et al.* Braun Lipoprotein (Lpp) Contributes to Virulence of Yersiniae:
796 Potential Role of Lpp in Inducing Bubonic and Pneumonic Plague. *Infect Immun*
797 2008;**76**:1390–409.

798 Shaffer CL, Zhang EW, Dudley AG *et al.* Purine Biosynthesis Metabolically Constrains
799 Intracellular Survival of Uropathogenic Escherichia coli. *Infection and Immunity*
800 2017;**85**, DOI: 10.1128/IAI.00471-16.

801 Shankar-Sinha S, Valencia GA, Janes BK *et al.* The Klebsiella pneumoniae O Antigen
802 Contributes to Bacteremia and Lethality during Murine Pneumonia. *Infect Immun*
803 2004;**72**:1423–30.

804 Short FL, Di Sario G, Reichmann NT *et al.* Genomic Profiling Reveals Distinct Routes To
805 Complement Resistance in Klebsiella pneumoniae. *Infect Immun* 2020;**88**, DOI:
806 10.1128/IAI.00043-20.

807 Sydenham M, Douce G, Bowe F *et al.* Salmonella enterica Serovar Typhimurium surA Mutants
808 Are Attenuated and Effective Live Oral Vaccines. *Infection and Immunity*
809 2000;**68**:1109–15.

810 Tacconelli E, Carrara E, Savoldi A *et al.* Discovery, research, and development of new
811 antibiotics: the WHO priority list of antibiotic-resistant bacteria and tuberculosis.
812 *Lancet Infect Dis* 2018;**18**:318–27.

813 The UniProt Consortium. UniProt: a worldwide hub of protein knowledge. *Nucleic Acids Res*
814 2019;**47**:D506–15.

815 Touati D. Iron and Oxidative Stress in Bacteria. *Archives of Biochemistry and Biophysics*
816 2000;**373**:1–6.

817 Treviño-Quintanilla LG, Freyre-González JA, Martínez-Flores I. Anti-Sigma Factors in E.
818 coli: Common Regulatory Mechanisms Controlling Sigma Factors Availability. *Curr*
819 *Genomics* 2013;**14**:378–87.

820 Vogel H, Altincicek B, Glöckner G *et al.* A comprehensive transcriptome and immune-gene
821 repertoire of the lepidopteran model host Galleria mellonella. *BMC Genomics*
822 2011;**12**:308.

823 Wand ME, Baker KS, Benthall G *et al.* Characterization of pre-antibiotic era Klebsiella
824 pneumoniae isolates with respect to antibiotic/disinfectant susceptibility and virulence
825 in Galleria mellonella. *Antimicrob Agents Chemother* 2015;**59**:3966–72.

826 Wang S, Blahut M, Wu Y *et al.* Communication between Binding Sites Is Required for YqjI
827 Regulation of Target Promoters within the yqjH-yqjI Intergenic Region. *J Bacteriol*
828 2014;**196**:3199–207.

829 Wang S, Wu Y, Outten FW. Fur and the Novel Regulator YqjI Control Transcription of the
830 Ferric Reductase Gene yqjH in Escherichia coli. *Journal of Bacteriology*
831 2011;**193**:563–74.

832 Washington-Hughes CL, Ford GT, Jones AD *et al.* Nickel exposure reduces enterobactin
833 production in Escherichia coli. *MicrobiologyOpen* 2019;**8**:e00691.

834 Wick RR, Heinz E, Holt KE *et al.* Kaptive Web: User-Friendly Capsule and
835 Lipopolysaccharide Serotype Prediction for Klebsiella Genomes. *Journal of Clinical*
836 *Microbiology* 2018;**56**, DOI: 10.1128/JCM.00197-18.

837 Wick RR, Judd LM, Gorrie CL *et al.* Unicycler: Resolving bacterial genome assemblies from
838 short and long sequencing reads. Phillippy AM (ed.). *PLoS Comput Biol*
839 2017;**13**:e1005595.

840 Wick RR, Schultz MB, Zobel J *et al.* Bandage: interactive visualization of de novo genome
841 assemblies. *Bioinformatics* 2015;**31**:3350–2.

842 Wyres KL, Lam MMC, Holt KE. Population genomics of Klebsiella pneumoniae. *Nature*
843 *Reviews Microbiology* 2020;**18**:344–59.

844 Xiong H, Carter RA, Leiner IM *et al.* Distinct Contributions of Neutrophils and CCR2+
845 Monocytes to Pulmonary Clearance of Different Klebsiella pneumoniae Strains.
846 *Infection and Immunity* 2015;**83**:3418–27.

847 Yeh K-M, Chiu S-K, Lin C-L *et al.* Surface antigens contribute differently to the
848 pathophysiological features in serotype K1 and K2 Klebsiella pneumoniae strains
849 isolated from liver abscesses. *Gut Pathog* 2016;**8**, DOI: 10.1186/s13099-016-0085-5.

850 Yu VL, Hansen DS, Ko WC *et al.* Virulence Characteristics of Klebsiella and Clinical
851 Manifestations of K. pneumoniae Bloodstream Infections. *Emerg Infect Dis*
852 2007;**13**:986–93.

853

854 Tables

855 **Table 1: Plasmid replicons in RH201207 identified by PlasmidFinder**

Plasmid	Identity	Query length / Template length	Contig	Position in contig	Accession number
ColRNAI	100 %	130 / 130	RH201207_8	10359-10488	DQ298019
IncFIB(K)	100 %	560 / 560	RH201207_7	4026-4585	JN233704
IncFIB(pQil)	100 %	740 / 740	RH201207_2	217-956	JN233705
IncFII(K)	97.8 %	148 / 148	RH201207_2	50275-50422	CP000648
IncFII(K)	97.8 %	148 / 148	RH201207_6	1728-1875	CP000648
IncX3	100 %	374 / 374	RH201207_5	32841-33214	JN247852

856

857 **Table 2: Unique insertion sites of the TraDIS libraries used**

Sample	Chromosome length	Unique Insertion Sites (UIS)	Length / UIS
RH201207	5,475,790 bp	510,834	10.72 bp
RH201207 2 hpi	5,475,790 bp	379,343	14.43 bp
RH201207 6 hpi	5,475,790 bp	359,602	15.23 bp
ATCC 43816	5,374,835 bp	415,608	12.93 bp
ATCC 43816 4 hpi	5,374,835 bp	350,363	15.34 bp

858